Molecular-dynamics simulations of collisions between energetic clusters of atoms and metal substrates

Horngming Hsieh* and R. S. Averback
Department of Materials Science and Engineering, University of Illinois at Urbana-Champaign, Urbana, Illinois 61801

Harrell Sellers
National Center for Supercomputing Applications, Beckman Institute for Advanced Science and Technology, University of Illinois, Urbana, Illinois 61801

C. P. Flynn
Department of Physics, University of Illinois at Urbana-Champaign, Urbana, Illinois 61801
(Received 31 July 1991)

The collisional dynamics between clusters of Cu, Ni, or Al atoms, with energies of 92 eV to 1.0 keV and sizes of 4 to 92 atoms, and substrates of these same metals were studied using molecular-dynamics computer simulations. A diverse behavior was observed, depending sensitively on the size and energy of the cluster, the elastic and chemical properties of the cluster-substrate combination, and the relative mass of the cluster and substrate atoms. For the 92-atom Cu clusters impacting a Cu substrate, the cluster can form a "glob" on the surface at low energy, while penetrating the substrate and heavily deforming it at high energies. When the cluster energy exceeds ≈ 25 eV/atom, the substrate suffers radiation damage. The 92-atom Al clusters do not much deform Ni substrates, but rather tend to spread epitaxially over the surface, despite the 15% lattice mismatch. For 1-keV collisions, several Al atoms dissociate from the cluster, either reflecting into the vacuum or scattering over the surface. 326-eV Ni clusters embed themselves almost completely within Al substrates and form localized amorphous zones. The potentials for these simulations were derived from the embedded-atom method, although modified to treat the higher-energy events. *Ab initio* linear-combination-of-atomic-orbitals–molecular-orbitals calculations were employed to test these potentials over a wide range of energies. A simple model for the expected macroscopic behavior of cluster-solid interactions is included as an appendix for a comparison with the atomistic description offered by the simulations.

I. INTRODUCTION

The interactions between energetic clusters and surfaces are of growing scientific interest because of their potential importance for such applications as surface metallization, surface cleaning, catalysis, cluster science, precision machining, and cluster fusion.[1–4] Ionized cluster beam (ICB) deposition, for example, has recently received a great deal of attention as a promising method for synthesizing high-quality thin films at low temperatures.[2] The basic idea motivating the use of energetic cluster beams for thin-film deposition is that a large amount of energy, some keV, can be delivered to a localized region of the surface where it can stimulate atomic motion. Such a localization of energy has been found helpful during ion-beam-assisted deposition (IBAD) in lowering the temperatures that are required for good epitaxial growth.[5] Among some possible drawbacks to IBAD, however, are its potential for creating radiation damage and the implantation of the irradiating species. In contrast to IBAD, no single atom in an energetic cluster under "typical" ICB conditions is expected to carry sufficient energy to become implanted or to create radiation damage in the underlying substrate. Rather, it is believed that the clusters either fragment or melt on impacting the surface and that cluster atoms undergo stimulated migration over the substrate surface. Our molecular-dynamics (MD) simulations revealed, however, that the cluster-substrate interaction is more complex than this simple picture affords, and that the collective nature of the collision must be considered to fully understand the deposition process.[6] It was demonstrated, for example, that a Cu cluster of 92 atoms and 326 eV can penetrate a Cu substrate by a shear deformation process, even though each atom in the cluster initially contains just 3.54 eV.

The experimental difficulties in studying cluster-solid interactions are numerous, as few techniques have both the lateral and depth resolution required to investigate single cluster impacts or the time resolution to capture the dynamics of these highly transient events. However, the problem of energetic clusters impacting surfaces is quite conducive to study by MD simulations; the volume of material affected by clusters of a few to hundreds of atoms, and energies up to several keV, is quite small, requiring less than $\approx 1\times 10^5$ atoms in a simulation cell, while the total time for the interaction is less than ≈ 10 ps. Moreover, the development of reliable interatomic potentials now makes it possible to address real systems with confidence. In an earlier study of cluster-solid in-

teractions, we had employed Lennard-Jones potentials,[7] and although this work provided some insight into the collective nature of the collision dynamics, it was not easy to relate these results to the behavior of real metal or semiconductor systems. The present simulations employ embedded-atom-method (EAM) potentials.[8,9] For some of the more energetic events, a hybrid potential consisting of EAM potentials plus the Molière potential was employed. In the development of our potentials we used *ab initio* linear-combination-of-atomic-orbitals–molecular-orbitals (LCAO–MO) calculations[10] to provide benchmarks for testing these potentials at close range.

In the current work, we will show that the way that a cluster interacts with a solid substrate depends on a number of parameters describing the cluster and substrate: these include the size and energy of the cluster, the elastic and chemical properties of the substrate and cluster, and the relative atomic masses of the cluster and substrate. Although the details of these interactions are complex, a simple macroscopic model can illustrate how these various parameters can influence cluster-substrate interactions. This model, which was developed by one of the authors (C.P.F.), is included as an appendix for comparison with the atomistic MD simulations.

II. THE SIMULATION MODEL

A. Interatomic potentials

The requirements of interatomic potentials employed for cluster-substrate interactions, and ion-beam modifications of materials in general, are rather severe, since the energies of the interactions range from under a tenth of an eV to more than some tens of eV. At the high end of the energy regime, pair potentials, such as the Moliere or universal potential,[11] are adequate, whereas at the low end, many-body potentials, such as those derived from the embedded-atom method, must be employed. To span the entire energy regime of relevant interactions, hybrid interatomic potentials were developed for the Cu cluster impacts by combining EAM potentials with a Moliere potential. The connection between the two potentials, which occurs over an energy regime from $\approx 20-100$ eV, was made by using a cubic spline fit between the Moliere potential and the repulsive pair potential in the EAM potentials. Over the same range, the cohesive part of the many-body potential is smoothly switched off. The choice for the screening length in the Moliere potential, as well as the details of the connection of the two potentials, is somewhat arbitrary; however, data of threshold energies for atomic displacements, i.e., the minimum energy required to create a Frenkel pair (FP), were employed as benchmarks for fitting. Threshold energies are generally anisotropic; in Cu they range from 20 to 80 eV.[12] Our hybrid potential, therefore, was adjusted by simulating dynamic recoil events that lead to atomic displacements. Shown in Table I are the results of the simulations for three recoil directions and three choices for the screening length in the Moliere potential (denoted as $L_{s,1}$–$L_{s,3}$). The bottom two rows contain experimentally determined threshold energies reported by

TABLE I. Threshold displacement energy anisotropy. Three recoil directions are included: 1° from ⟨111⟩, 1° from ⟨100⟩, and $\theta=67.5°$ and $\phi=0°$. For each direction, three screening lengths in the Moliere potential were tested: $L_{s,1}=0.0738$, $L_{s,2}=0.0960$, and $L_{s,3}=0.088\,26$. 0, 1, or 2 indicate the number of FP's produced. The bottom two rows are simulation data from Refs. 12 and 13.

	1° [111] $\theta=44.74°$ $\phi=45°$			1° [100] $\theta=89°$ $\phi=0°$			$\theta=67.5°$ $\phi=0°$		
Recoil Energy (eV)	$L_{s,1}$	$L_{s,2}$	$L_{s,3}$	$L_{s,1}$	$L_{s,2}$	$L_{s,3}$	$L_{s,1}$	$L_{s,2}$	$L_{s,3}$
15				0					
20						0			
25				1	0	1			
30					1				
35	0				1				
40	1								
45									
50	1								0
55								0	1
60									
65								1	1
70			0						
75			0						
80		0	1					2	
85									
100		0							
120		0							
130		1							
Ref. 12		75 eV			20 eV			65 eV	
Ref. 13		80 eV			25 eV			40 eV	

King and Benedek.[12] Also shown, for comparison, are MD simulation data obtained by Gibson *et al.* using the Gibson II potential.[13] The table shows that the Moliere potential with a screening length of $L_s = 0.088\,26$ provides the best match to the experimental data.

Ab initio LCAO–MO calculations[10] were also employed to set benchmarks for testing the interatomic potentials at close range. This application of LCAO–MO should prove extremely important, since the use of experimental displacement energies is limited. These values are statistical quantities, whereas, for practical reasons, few simulations around a given symmetry direction can be run. Moreover, displacement energies in most metals are known only imprecisely. Figure 1 illustrates the model calculation; a cluster of eight atoms is created with each atom initially located at its perfect crystal lattice site; a single atom, atom *A*, is then moved along the [110] direction toward atom *B*. The potential energy of the system is calculated at selected distances. Because atom *A* approaches atom *B* in the presence of the other nearest-neighbor atoms, the potential reflects the many-body effects. In addition, atom *A* can be different from the other seven atoms, so that alloys can be studied by this scheme.

The curves in Fig. 2 show the potential energy of the system of eight atoms as a function of distance between atoms *A* and *B* obtained by the hybrid potential, the EAM potential,[8] and the LCAO–MO calculation. The three sets of data were normalized at the nearest-neighbor distance r_b, which is 2.55 Å for Cu. The results show that the benchmarks set by the *ab initio* LCAO–MO calculations lie on the curve of the hybrid potential. One of the calibration points has a potential energy of 675 eV at a distance of 0.638 Å, whereas the hybrid potential yields 468 eV at this separation. Although this discrepancy is not significant for the interactions studied here, where the relevant atomic energies are significantly below ≈ 100 eV, it would be important for calculations of defect production.

For the Al and Ni system, the EAM potentials of Voter and Chen were employed.[9] These potentials are similar to those of Foiles, Baskes, and Daw,[8] except that they employ a Morse potential for the repulsive ion-ion interaction. Since the Morse potential also contains an attractive part, the Voter-Chen potential is not completely dependent on the embedding function for cohesion. The LCAO–MO calculations were employed to check these potentials as well; the results are shown in Fig. 3. For Ni or Al atoms approaching the seven fixed Ni lattice atoms, the calibration points lie close to the EAM curve, although the interaction between the Al atom and seven Ni atoms (the dashed line) is somewhat "softer" than that for the pure Ni case. The results for the Al matrix are shown in Fig. 4. The LCAO–MO data are shifted slightly to smaller separations, implying a smaller "hard-core" radius. Again, we remark that these deviations are not overly significant for the cluster-substrate collisions studied here, where the initial energy per atom

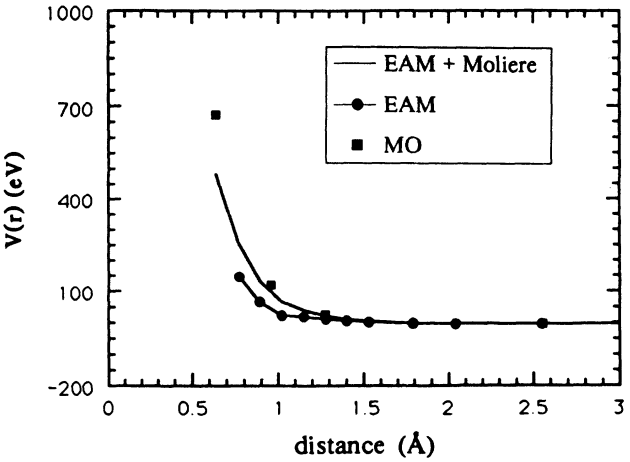

FIG. 2. Changes of potential relative to the distance between atoms *A* and *B* in Fig. 1. The three sets of data are the results from the hybrid potential (solid line), the EAM potential (dashed line), and the molecular-orbital calculations (squares).

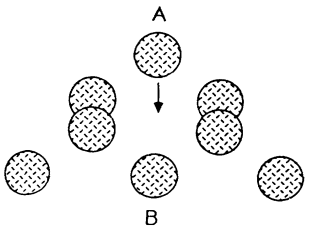

FIG. 1. A cluster of eight atoms at their lattice sites. Atom *B* is the nearest-neighbor atom of the other seven atoms. Atom *A* approaches atom *B* along [110], while the other atoms are fixed. The system is used to calculate the changes of potential relative to the interatomic distances.

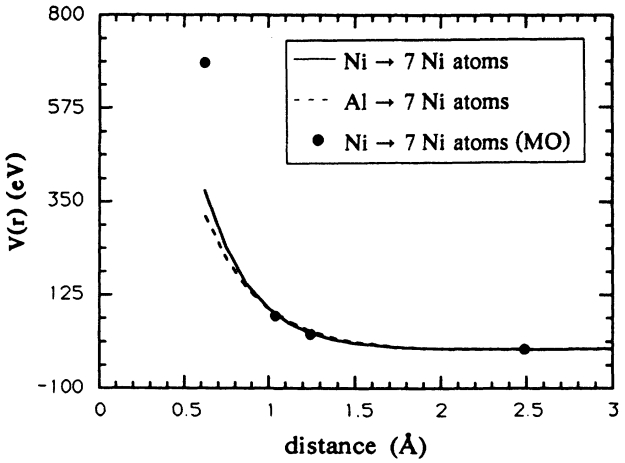

FIG. 3. Changes of potential relative to the distance between atoms *A* and *B* in Fig. 1. The Ni-7Ni curve is the data for atom *A* and the others being Ni atoms. The Al-7Ni curve is the data for atom *A* being Al and the others being Ni. The circles are the results from molecular-orbital calculations.

in the Ni cluster is 3.26 eV, but for other beam-assisted deposition and radiation damage problems, the Chen-Voter potential would need modification. A more-detailed description of the use of the LCAO–MO method for generating empirical potentials will be published elsewhere.[14]

B. The simulation system

The MD simulations in this work are fully dynamical, three-dimensional calculations. The orthorhombic substrates had dimensions $19a_0 \times 19a_0 \times 11a_0$ (a_0 is the lattice parameter), except for the 92- and 326-eV Cu clusters impinging on a Cu substrate [denoted as Cu_{92}(92 eV)→Cu and Cu_{92}(326 eV)→Cu, respectively], where the dimensions were somewhat smaller, $11a_0 \times 11a_0 \times 5a_0$. Two layers of damped atoms were employed inside fixed boundaries on five of the faces, with damping coefficients adjusted to mimic the flow of vibrational energy from the region of the computational cell to a semi-infinite surrounding medium. No constraints or damping were placed at the substrate surface, which was (001). The incident clusters were approximately spherical, but they were relaxed prior to initiating the event. For convenience, the cluster and the substrate were crystallographically aligned at the outset; however, the cluster velocity was directed 9° from the surface normal to avoid singular behavior. The tangential velocity was in the [110] direction.

III. IMPACT OF Cu CLUSTERS ON Cu AND Ni SUBSTRATES

We begin our discussion of cluster-solid collisions by describing the interactions between Cu clusters and Cu or Ni substrates. These collisions were employed to investigate the influence of the size and energy of the cluster and the relative elastic properties of the cluster and substrate. EAM potentials for Cu and Ni were obtained from Ref. 8. The general features of the interaction between a large cluster of atoms with a substrate can be clearly seen in Figs. 5(a) and 5(b), which show snapshots of the atoms in the simulation cell at various instants of

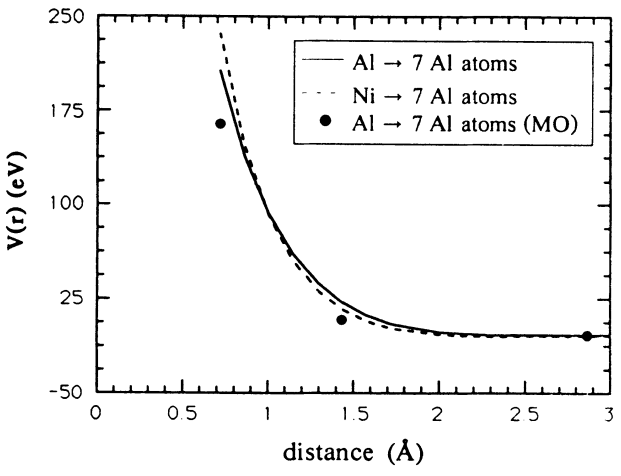

FIG. 4. Changes of potential relative to the distance between atoms *A* and *B* in Fig. 1. The Al-7Al curve is the data for atom *A* and the others being Al atoms. The Ni-7Al curve is the data for atom *A* being Ni and the others being Al. The circles are the results from molecular-orbital calculations.

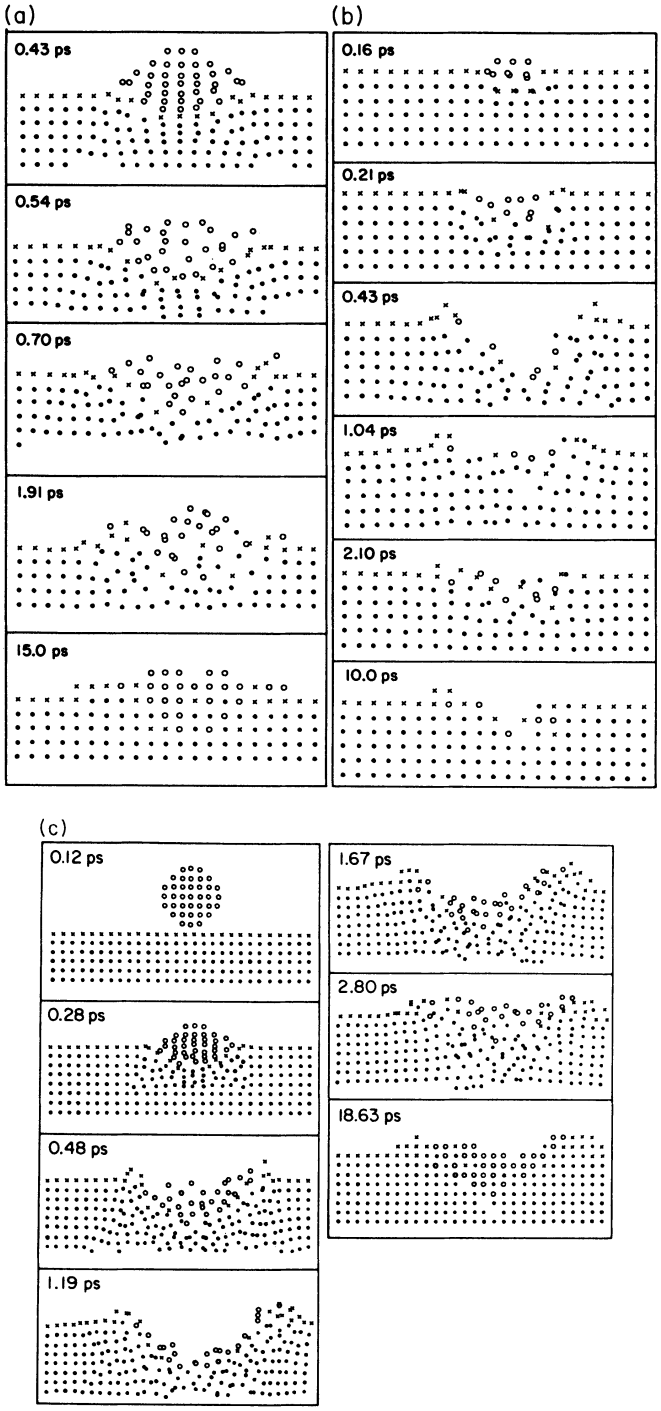

FIG. 5. Sequential snapshots of the locations of cluster atoms (○), surface atoms in the substrate (×), and other substrate atoms (●) at various instants of time into the event. (a) Cu_{92}(326 eV)→Cu; (b) Cu_{92}(326 eV)→Ni; (c) Cu_{92}(1.0 keV)→Cu.

time during a collision event between Cu_{92}(326 eV) with either a Cu substrate [Fig. 5(a)] or Ni substrate [Fig. 5(b)]. For clarity, only atoms within a cross-sectional slab containing two (200) planes through the center of the cluster are shown. As the impact begins, the atoms in the cluster-substrate interface begin to compress, with the cluster losing its crystalline structure as it massively deforms. This occurs on a time scale of one lattice vibration and should not be identified with local heating and subsequent melting, but rather as a dynamic shearing of the cluster and substrate material. During these initial stages of the collision, the cluster depresses the substrate surface, but surface and cluster atoms do not interpenetrate each other; i.e., intermixing is small. This observation confirms that some of the gross features of the interaction can be viewed on a macroscopic level, without consideration of the details of the atomic collision processes (see the Appendix). After the initial elastic-plastic compression of the substrate at ≈ 0.68 ps, the impacted region starts to rebound upward, but no atoms are reflected from the surface. At ≈ 1.02 ps, the system is near its maximum expansion, and substrate atoms begin to appear on the surface at the periphery of the cluster. Still, little intermixing of cluster and substrate is observed. By 2.40 ps into the event, the atoms begin to relax to their final equilibrium locations, with many cluster atoms replacing the substrate atoms in the near surface. Within 5.47 ps of the impact, the system has almost completely relaxed, and all atoms settle onto lattice sites.

The locations of cluster atoms at the end of the event are shown in the top and side views in Fig. 6. Here, all atoms in an atomic row are included in the projected views. For the Cu substrate, Fig. 6(a) (middle) shows that the cluster atoms form two epitaxial layers on the surface and that they extend in depth to the third (200) plane. The complete depth distribution of cluster atoms is compiled in Table II. The top view shows the spreading of atoms over the surface. No evidence for fragmentation of the cluster is apparent. Only a few cluster atoms do not have at least one other cluster atom as a nearest neighbor, and of these, all are within the cutoff distance of the potential from another cluster atom, 4.95 Å. Cluster atoms do, however, spread over the surface; the radius of gyration r_g of those cluster atoms in the epilayers is $2.236a_0$ (values of r_g for all events are listed in Table III). [$r_g = (\langle r_i^2 \rangle)^{1/2}/N$, where r_i is the transverse distance between the ith cluster atom and the center of mass of the N cluster atoms in the epilayers.] This compares to $r_g = 1.096a_0$ for the original cluster. Atoms most distant from the center of the cluster come from surface sites on the central equatorial planes of the cluster, illustrating that during the rapid compression of the cluster, these atoms shear from the cluster as it penetrates the substrate.

The spatial distribution of substrate atoms that are transported onto the surface also provides a revealing

TABLE II. The number of cluster atoms, the number of vacancies, and the number of interstitials at every atomic layer at the end of the event. s_i is the ith substrate layer below the surface ($i=1$ is the surface layer) and e_i is the ith epilayer above s_1. For Al_{92}(1.0 keV)→Ni, three cluster atoms are reflected from the surface.

	e_3	e_2	e_1	s_1	s_2	s_3	s_4	s_5	s_6	s_7	s_8	s_9	s_{10}	s_{11}
Cluster atoms														
Cu_{92}(326 eV)→Cu		10	50	20	9	3								
Cu_{92}(326 eV)→Ni		18	60	14										
Cu_{92}(1.0 keV)→Cu		4	18	29	21	15	3	1	1					
Al_{92}(326 eV)→Ni		1	69	20	2									
Al_{92}(1.0 keV)→Ni			49	27	12	1								
Cu_{92}(92 eV)→Cu	10	33	44	4	1									
Cu_{13}(326 eV)→Cu			1	4	7	1								
Cu_4(326 eV)→Cu					3		1							
Vacancies														
Cu_{92}(326 eV)→Cu														
Cu_{92}(326 eV)→Ni					1									
Cu_{92}(1.0 keV)→Cu				4		1	1	1	1	1				
Al_{92}(326 eV)→Ni														
Al_{92}(1.0 keV)→Ni				2	1			1						
Cu_{92}(92 eV)→Cu														
Cu_{13}(326 eV)→Cu				7	1									
Cu_4(326 eV)→Cu				10	1	2								
Interstitials														
Cu_{92}(326 eV)→Cu														
Cu_{92}(326 eV)→Ni														
Cu_{92}(1.0 keV)→Cu														
Al_{92}(326 eV)→Ni														
Al_{92}(1.0 keV)→Ni														
Cu_{92}(92 eV)→Cu														
Cu_{13}(326 eV)→Cu														
Cu_4(326 eV)→Cu											1	1	1	1

picture of the collision dynamics. It is seen in Figs. 6(a) (bottom) and 6(b) (bottom) that these atoms form a ridge surrounding the impact zone. We can infer from this distribution and Fig. 5 that the shear stress generated in the substrate exceeded its critical shear strength. Thus, during the compression stage of the impact, atoms below the cluster shear relative to those just outside the impact zone. On subsequent expansion, substrate atoms at the perimeter of the cluster flow onto the surface. A similar picture is obtained on viewing the flow of atoms on an atomic level. In Fig. 7, several representative atomic displacement trails that bring substrate atoms onto the surface are illustrated. The figure was constructed by locating substrate atoms that were transported to the surface, and backtracking to find which atoms acquired their lattice sites, and which atoms, in turn, replaced them. The trails were traced back to where a cluster atom made the replacement; this site is identified in the figure. It is ob-

TABLE III. The radii of gyration of the cluster atoms. Left column shows the radii of gyration of all cluster atoms. Right column shows the radii of gyration of cluster atoms in the epilayers, only. Unit are lattice constants a_0. The radius of gyration of a 92-atom cluster before deposition is $1.096a_0$, that of a 13-atom cluster is $0.554a_0$, and that of a four-atom cluster is $0.354a_0$. Cluster atoms in events $G-I$ are embedded in the substrate, so values for epilayers are not applicable.

	r_g (total)	r_g (epilayers)
Cu_{92}(326 eV)→Cu	1.986	2.236
Cu_{92}(326 eV)→Ni	2.229	2.383
Cu_{92}(1.0 keV)→Cu	2.049	2.821
Al_{92}(326 eV)→Ni	3.044	3.331
Al_{92}(1.0 keV)→Ni	5.306	6.737
Cu_{92}(92 eV)→Cu	1.753	1.780
Cu_{13}(326 eV)→Cu	1.004	
Cu_4(326 eV)→Cu	0.680	
Ni_{92}(326 eV)→Al	1.405	

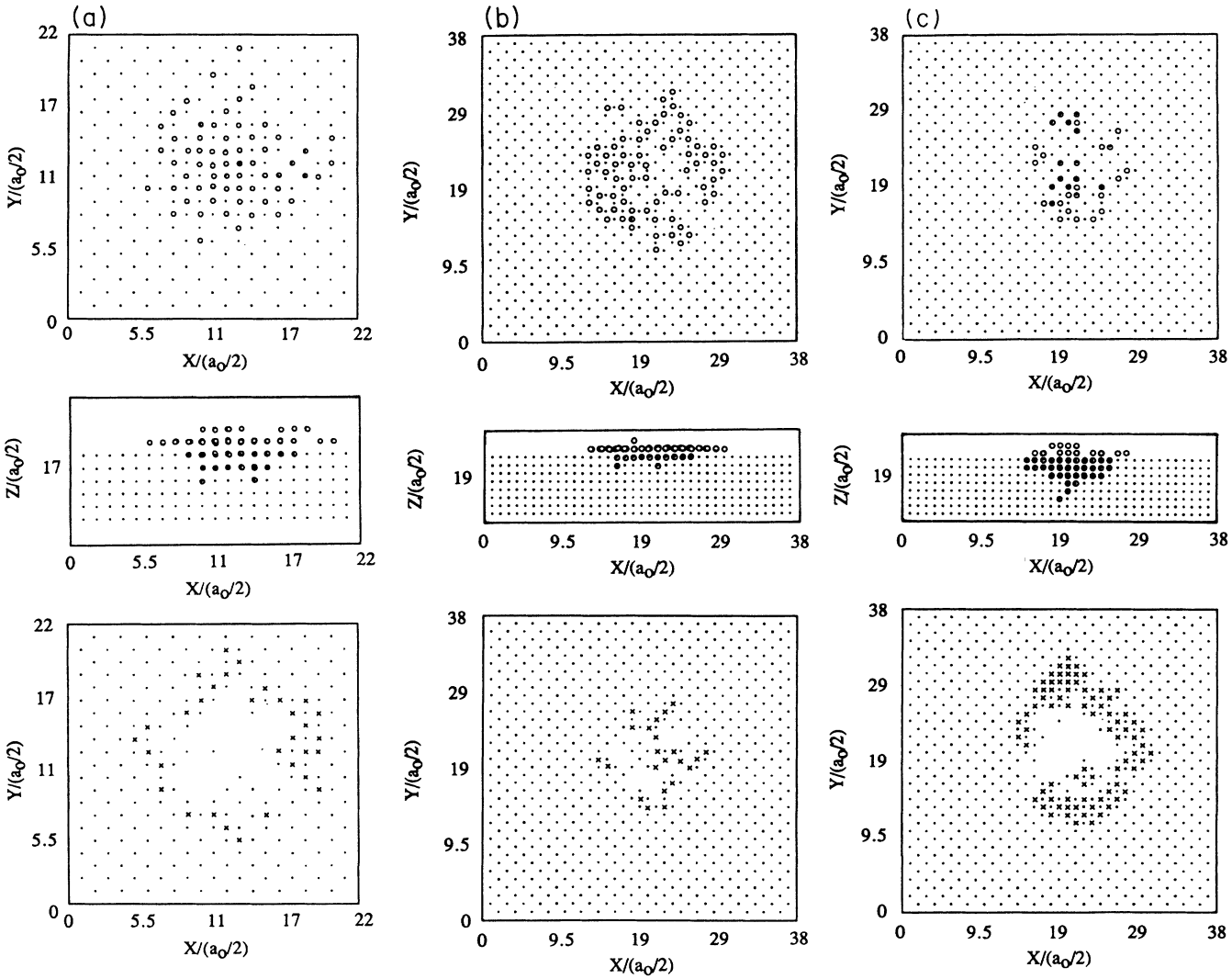

FIG. 6. The locations of atoms at the end of the event. Top: top view of cluster atoms (○) on the surface; middle: side view of all cluster atoms (○); bottom: top view of substrate atoms (×) on the surface and substrate atoms (·) in the surface layer. (a) Cu_{92}(326 eV)→Cu; (b) Cu_{92}(326 eV)→Ni; (c) Cu_{92}(1.0 keV)→Cu.

served that substrate atoms move radially outward and then flow upward onto the surface. Although some of the sequences cover several atomic distances, any single atom moves only about one atomic distance; thus these displacement trails are comprised of replacement sequences. These sequences, however, are distinguished from replacement collision sequences (RCS's), which are familiar in the field of radiation damage.[13] RCS's are linear trails of replacement events propagating at supersonic velocities and are responsible for the creation of point defects (Frenkel pairs) during particle irradiation. The replacement events here are not linear; they travel at subsonic speeds, and no Frenkel pairs are created.

Similar behavior is observed when Cu_{92}(326 eV) impacts a Ni substrate, as illustrated in the sequence of Figs. 5(b) and 6(b). Important differences, however, are apparent. For example, Fig. 6(b) and Tables II and III show that the penetration of the Cu cluster is less in Ni. Whereas 35% of the cluster atoms are embedded in the Cu substrate, only 15% are embedded in the Ni substrate, and just one Cu cluster atom penetrates deeper than the surface layer. The value of r_g for this case is $2.383a_0$, which is somewhat larger than the case of Cu_{92}(326 eV)→Cu. A ridge of substrate atoms is still created on the Ni substrate, but here it is less pronounced. No Frenkel pairs are produced in this event, but a single vacant site is created in the second substrate layer. With only one vacancy, and a single collision event, it is uncertain whether this observation signifies a real difference between the response of Cu and Ni substrates or is just a statistical artifact. It is consistent, however, with the overall more rigid response of the Ni substrate, which would not allow time for defect recovery. We attribute this more rigid response to the higher strength of Ni, since kinematic and chemical factors should not be significant.

The effect of increasing the cluster energy on the interaction is seen in Figs. 5(c) and 6(c), where the impact of Cu_{92}(1.0 keV)→Cu is illustrated. At this higher energy, the plastic response of the substrate becomes far more pronounced. At 1.19 ps, the cluster has depressed the substrate to the extent that the cluster itself has dipped below the original surface. Similar to the 326-eV events, however, no substantial intermixing between the cluster and substrate is observed during the compression stage, and no RCS's are generated. Substrate atoms respond to the stress rather by flowing around the cluster and onto the surface, where now a well-defined ridge of atoms is formed [Fig. 6(c)]. At the end of the event, 70 of the 92 cluster atoms are embedded in the substrate, while 79 substrate atoms are brought onto the surface. Nine va-

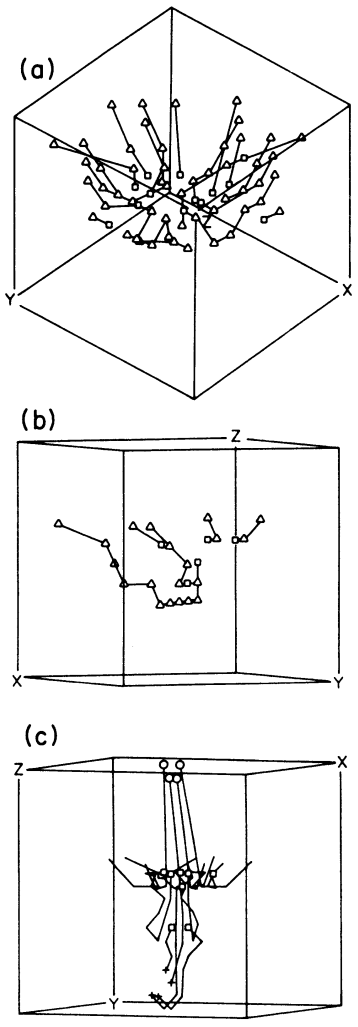

FIG. 7. Representative traces of atomic displacement sequences of substrate atoms that eventually end up on the surface, or as interstitial atoms. (a) Cu_{92}(326 eV)→Cu; (b) Cu_{13}(326 eV)→Cu; (c) Cu_4(326 eV)→Cu. Small squares locate where the substrate atom is first replaced by a cluster atom in (a) and (b); in (c) the squares show where displacement sequences were initiated whether they where induced by recoil or cluster atoms. Among them, four sequences end up as interstitials (+).

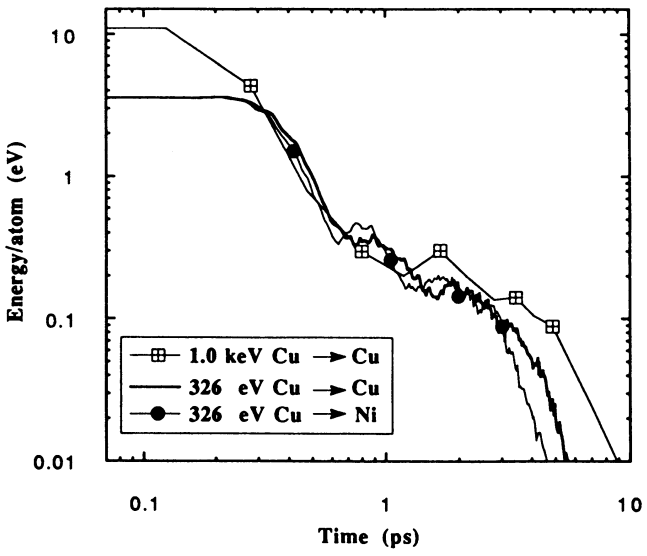

FIG. 8. Kinetic energies of cluster atoms as a function of time.

cancies are created, one as deep as the seventh layer below the surface. Since no RCS's or interstitials are generated, these vacancies appear to be a consequence of a rapid quenching of a localized melt zone, as is now discussed.

Snapshots of the 1-keV event at 1.67 and 2.80 ps suggest that, in addition to shearing, the substrate undergoes local melting. This is indicated by the apparent loss of crystalline structure over a wide band surrounding the cluster and by the interdiffusion between cluster and substrate atoms. These times, moreover, are sufficiently long and the heated volume sufficiently large that the concept of a liquid droplet is sensible. Macroscopic modeling confirms that a 1.0-keV cluster of 92 atoms falls within the parameter space where local melting is expected (see Appendix). To probe the local temperature in the vicinity of the cluster more carefully, the kinetic energies of the cluster atoms were followed in the simulations as a function of time; the results are shown in Fig. 8. In all three events, the kinetic energy drops rapidly during the initial compression stage. This is a consequence of compressing the local volume of material, heating the cluster and surrounding substrate, and possibly emitting shock waves. The 1-keV cluster loses kinetic energy at a much faster rate than the two lower-energy events, so that when the three events thermalize, the cluster atoms have similar kinetic energies, $\approx 0.1-0.4$ eV. The cluster atoms for the 1-keV event, however, cool more slowly, owing to the larger volume of surrounding substrate that has been heated. The kinetic energy of the cluster atoms over the time period of a few ps (i.e., some tens of lattice vibrations) is $\approx 0.1-0.4$ eV/atom or $\approx 800-3200$ K. These temperatures appear too low for melting any significant volume of the Ni substrate for as long as 1 ps, but they are high enough to melt Cu. For the 1-keV event, this is evident in Fig. 5(c). These data suggest, therefore, that the onset of significant melting in Cu substrates occurs at cluster energies of $\approx 0.5-1$ keV. It is worth noting that local melting in Cu during ion implantation also begins when ion energies reach ≈ 1 keV.[15] It signifies that for an energy pulse spreading in Cu for a few ps with a lattice thermal diffusivity of $\approx 10^{14}$ Å^2/s, 1 keV of energy is required to raise the temperature of the heated volume to its melting temperature. In contrast to the 1-keV cluster, a 92-eV cluster, Cu_{92}(92 eV)$\rightarrow$Cu, interacts rather weakly with the substrate. Although an energy of 1 eV/atom corresponds to a high thermal energy, the rapid transfer of this energy to the substrate prevents local melting. As seen by the distribution of cluster atoms in Table II, and the value of $r_g = 1.780a_0$, this cluster forms a "glob" on the surface without significant wetting or penetration.

The effect of cluster size was investigated by comparing collision events for Cu clusters containing 92, 13, or four atoms, impinging on Cu substrates with 326 eV. The energies per atom in the latter two clusters, 25.1 and 81.5 eV/atom are too large to use the Foiles-Daw-Baskes EAM potential;[8] thus the hybrid potential described in Sec. II was employed. For Cu_{92}(326 eV), which was described above, some cluster atoms substitute for substrate atoms and thus force other substrate atoms onto the surface; no vacancies or interstitial atoms are created in the substrate. For Cu_{13}(326 eV), a crater of eight vacancies is formed at the surface, but with no interstitials being created. Most of the cluster atoms are embedded in the substrate (see Table II). For Cu_4(326 eV), a crater is also formed, and all cluster atoms are embedded in the substrate. In addition, four interstitial atoms are created deep within the substrate—between the eighth and 11th atomic layers below the surface. In this regime, the response of the substrate switches from predominantly "elastic-plastic" to one of "radiation damage." This change in character in the cluster-substrate interaction can be seen by following the atomic displacement sequences shown in Fig. 7. For the Cu_{13}(326 eV)$\rightarrow$Cu, displacement chains terminate on the surface of the substrate, as shown in Fig. 7(b), which are similar to those for the Cu_{92}(326 eV) in Fig. 7(a), although some begin with replacements moving downward, into the substrate. For Cu_4 (326 eV)$\rightarrow$Cu, Fig. 7(c) shows that many recoil sequences are generated by the four cluster atoms. Among them, four replacement sequences extend into the substrate and terminate as interstitial atoms. It is noteworthy that "radiation damage" switches on for cluster energies of ≈ 25 eV/atom, which is approximately the threshold energy for defect production for single-particle collisions. In another event, a single atom was accelerated to 326 eV. Then, two vacancies were created in the fourth and sixth layers, and three interstitials (including the projectile) were produced: one in the fourth layer and two in the tenth layer. In regard to this event of a single-atom "cluster," it should be noted that when the number of atoms in the cluster becomes small, each event becomes less typical, and statistical averages over many directions become necessary. For this reason, the results of this event are not included in Table II. It should be noted, however, that the purpose here has not been to obtain accurate predictions of defect production, but rather to elucidate the mechanisms that operate in various regimes of cluster-solid interactions.

TABLE IV. Relevant properties for cluster-substrate interactions.

Target	Shear module (10^{12} erg/cm^3)	Nearest neighbor (Å)	Cohesive energy (eV)	Melting temperature (K)
Al	0.27	2.86	3.39	932
Ni	0.95	2.49	4.44	1725
Si	0.68	2.35	4.63	1700
Cu	0.55	2.55	3.49	1358

IV. IMPACTS OF Al CLUSTERS ON A Ni SUBSTRATE AND A Ni CLUSTER ON AN Al SUBSTRATE

The impacts of Al and Ni clusters on Ni and Al substrates, respectively, were simulated to further investigate the role of cohesive properties on cluster-solid collisions and also to explore the effects of chemical interactions and differences in the atomic masses of the cluster and substrate atoms. Three events are simulated: Al_{92}(326

eV)→Ni, Al_{92}(1.0 keV)→Ni, and Ni_{92}(326 eV)→Al. The time sequences of these events and the final locations of atoms are shown in Figs. 9(a)–9(c) and 10(a)–10(c), respectively. Quite remarkable is the enormous difference in behavior when Ni clusters strike Al or Al clusters strike Ni. While Ni_{92}(326 eV) completely embeds itself in Al, and intermixes with it, very little penetration and mixing is observed for the Al cluster impacting Ni, even when the cluster energy is raised to 1 keV. Note that at the instant of greatest compression, $t=0.34$ ps, the 1-keV Al cluster only slightly depresses the surface of the Ni substrate. Because of this rather small penetration, the ridge of substrate atoms surrounding the cluster impact that was characteristic of the Cu cluster impacts is not observed here [Figs. 10(a) and 10(b)].

The spreading of Al atoms over the Ni substrate is greater than the corresponding events for Cu clusters; $r_g=3.331a_0$ (a_0 of Ni) for the 326-eV event as compared to $r_g=2.236a_0$ and $2.383a_0$ For Cu_{92}(326 eV) on Cu and Ni, respectively. The value of r_g thus increases with increasing hardness of the substrate relative to the cluster. The larger value of r_g stems mostly from the small amount of cluster penetration. For example, only 22 Al atoms are embedded in the Ni substrate for the 326-eV event, leaving 70 Al atoms to be accommodated on the surface, and these (less one) lie in a single layer. Like the Cu_{92}(326 eV) on Ni event, the Al cluster does not dissociate. The one Al epilayer is seen to be perfectly epitaxial on the Ni substrate, even though the lattice parameter of Al has a ≈15% misfit with Ni. For Al_{92}(1.0 keV), Al atoms in the epitaxial layer have a much larger value of $r_{g'}=6.737a_0$; this larger value is indicative of a new mechanism coming into play, the dissociation of Al atoms from the main cluster and their scattering over the surface. Figure 11 illustrates the dissociation process by mapping some typical trajectories of cluster atoms that have sheared from the main cluster. The top view in Fig. 11 shows that the atoms leaving the cluster were initially on the central equatorial planes of the cluster, while the side view in Fig. 11 shows that atoms dissociate almost immediately on impact, within 0.1–0.2 ps. Two atoms are reflected from the surface as a dimer, and another cluster atom leaves the surface as a monomer. Other trajectories show that the dissociated atoms are initially

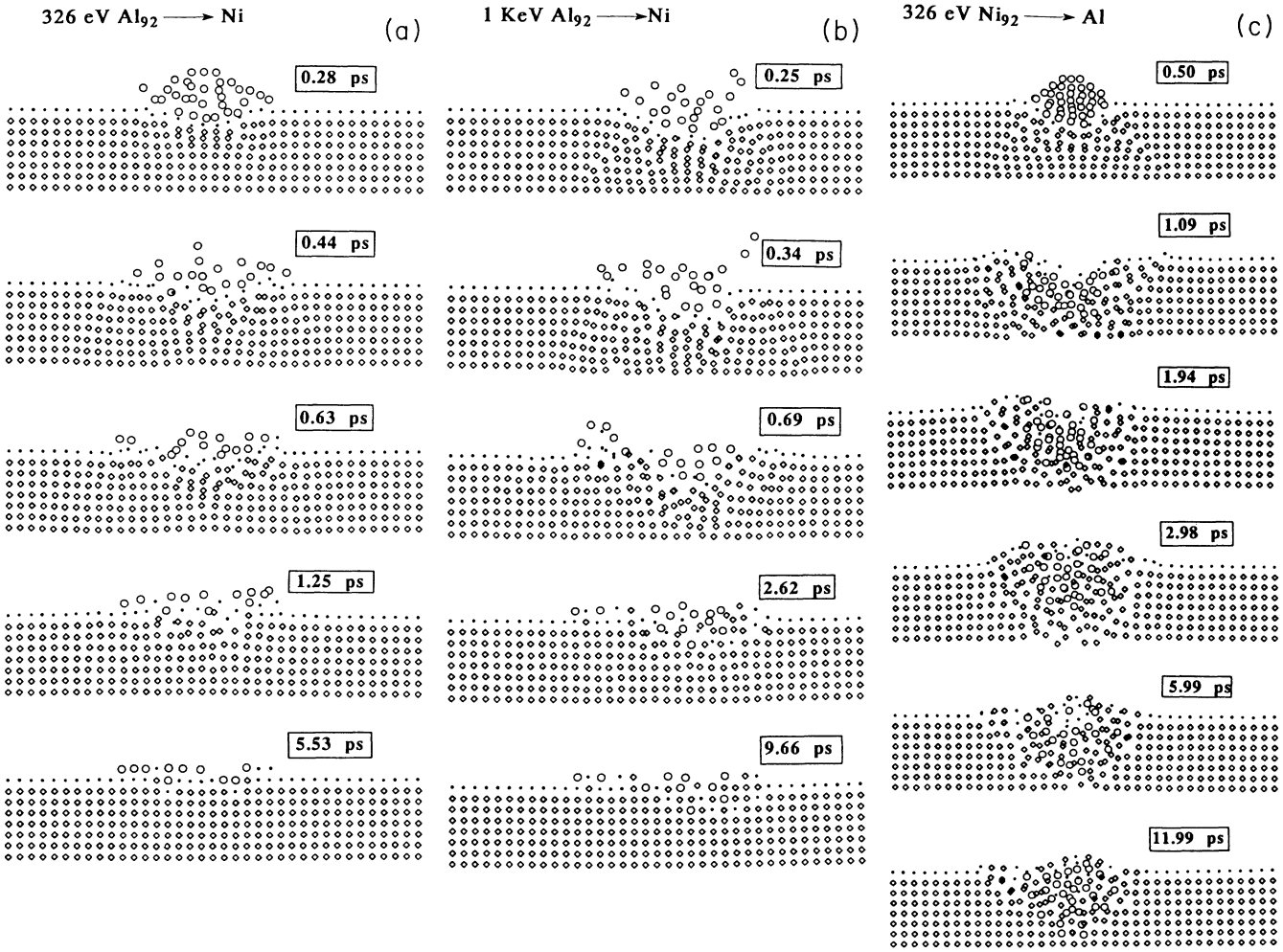

FIG. 9. Sequential snapshots of the locations of cluster atoms (○), surface atoms in the substrate (·) and other substrate atoms (◇) at various instants of time into the event. (a) Al_{92}(326 eV)→Ni; (b) Al_{92}(1.0 keV)→Ni; (c) Ni_{92}(326 eV)→Al.

reflected upward and radially outward, but since they cannot overcome the binding energy of the surface, they return to the surface. In some cases they "bounce." One trajectory, indicated by the symbol (○) in Fig. 11, is seen to scatter into a ⟨110⟩ channel during the bounce. These low orbits above the surface explain how cluster atoms can travel far distances over the surface. These atoms are clearly not migrating by a thermally stimulated diffusion process in this 0-K simulation.

The threshold energy for cluster dissociation is found, from these simulations, to lie between 326 eV and 1 keV for Al_{92} on Ni. This corresponds to 1.05–3.21 times the cohesive energy of Al, which is not surprising. However, the ratio of the initial kinetic energy of the cluster to its cohesive energy is not the only factor important for cluster dissociation; the relative cohesive energies of the cluster and substrate must also be considered. Note that the dynamics of 1 Cu_{92}(1.0 keV)→Cu is dramatically different from that of Al_{92}(1.0 keV)→Ni, yet the cohesive energy of Cu is not far different from that of Al (see Table IV). The reason for this difference is that the hard Ni substrate does not undergo substantial yielding under the Al cluster impact, thus making the substrate response far more elastic. The Al cluster rebounds from the surface at 0.2–0.3 ps when the cluster still contains 3–4 eV/atom, Fig. 12. The 1-keV Cu cluster, on the other hand, penetrates deeply into the Cu substrate and dissipates energy as it deforms and heats the substrate. The system does not begin to rebound upward until ≈1.2 ps when the kinetic energy of the cluster is only ≈0.3 eV/atom. In addition, when the Cu cluster atoms do rebound upward, they are constrained from moving outward by the surrounding matrix. Al atoms on the equatorial plane of the cluster surface; however, are not embedded in the Ni, and therefore they are not constrained by the Ni substrate; they can dissociate without obstruction. Thus, the relative cohesive energies of the cluster and substrate play an important role in determining the collision dy-

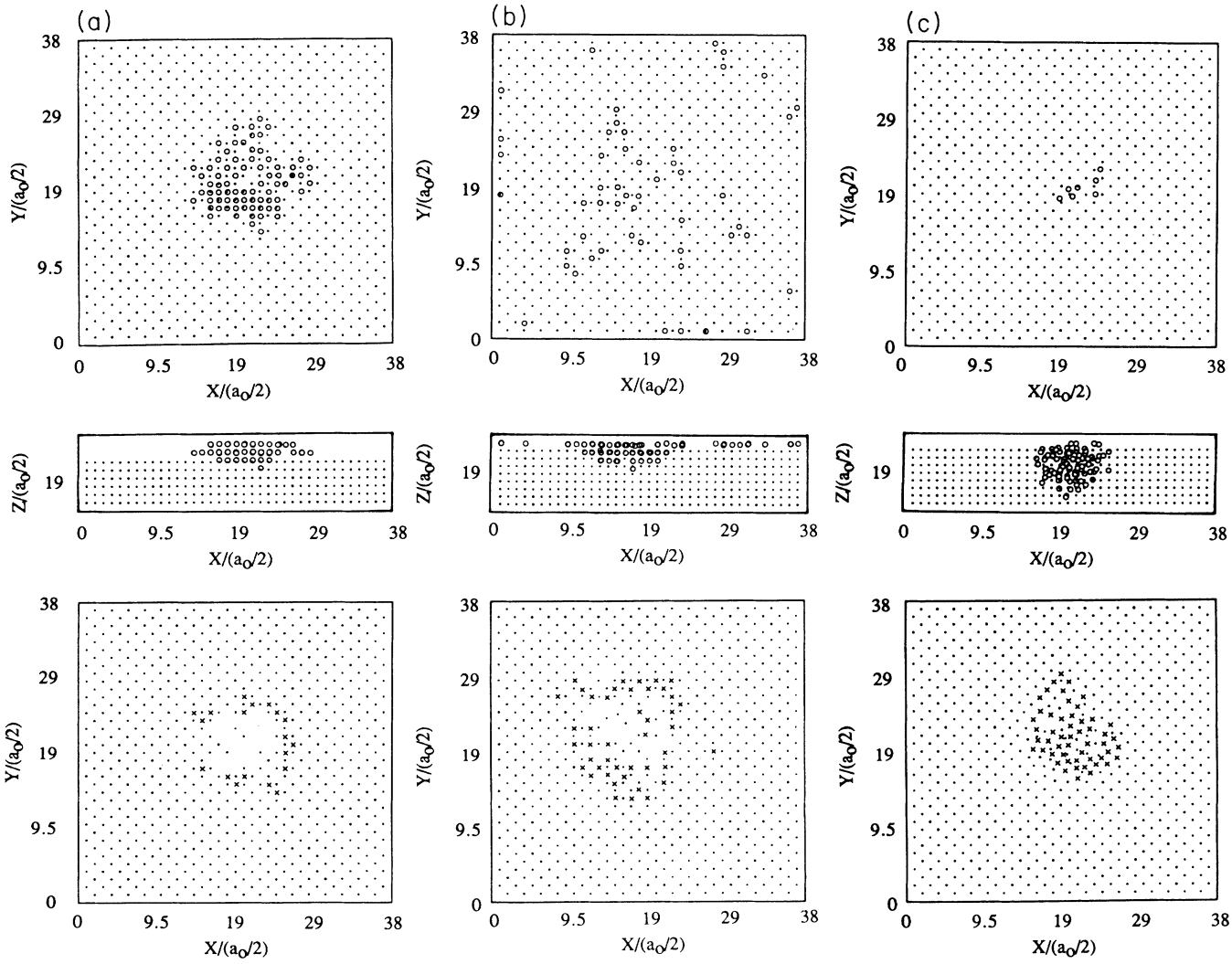

FIG. 10. The locations of atoms at the end of the event. Top: top view of cluster atoms (○) on the surface; middle: side view of all cluster atoms (○); bottom: top view of substrate atoms (×) on the surface and substrate atoms (·)in the surface layer. (a) Al_{92}(326 eV)→Ni; (b) Al_{92}(1.0 keV)→Ni; (c) Ni_{92}(326 eV)→Al.

namics. (As discussed in the Appendix, the shear modulus of the substrate is probably more relevant than its cohesive energy, but the latter is more convenient for comparison to the cluster; moreover, it tends to scale with the shear modulus.) A comparison of Cu_{92}(326 eV)→Ni with Al_{92}(326 eV)→Ni [Table II and Figs. 5(b), 6(b), 9(a), and 10(a)] shows that these collisions are very similar, although the Al spreads more widely over the Ni surface and the Ni substrates yields more to the Cu cluster. These small differences can be due to the differences in (i) the cohesive energies, (ii) atomic masses, or (iii) chemical affinities of Cu and Al for Ni. These studies show, therefore, that when the cohesive energies of clusters are equal to or greater than that of the substrate they impact, the clusters will embed themselves in the substrate and not dissociate. For larger sizes and higher energies, it may be possible that the cluster and substrate thermally vaporize, as discussed in the Appendix. That phenomenon, however, was not observed in the events studied here. Finally, for the energies and cluster sizes considered here, sputtering of the substrate does not occur.

For Ni_{92}(326 eV)→Al, Figs. 9(c) and 10(c) show that the interaction is substantially different from that of the other events. In this case, the cluster almost completely embeds itself in the Al; only seven Ni atoms remain above the surface layer. In addition, this event does not show a ridge of substrate atoms surrounding the cluster crater. Instead, the substrate atoms that are forced to the surface are nearly uniformly distributed over the impact zone. It also appears in Figs. 9(c) and 10(c) that the Ni and Al undergo substantial interdiffusion during the embedding process and that the local volume containing the cluster becomes amorphous. These latter two observations are examined more rigorously in Fig. 13, where the partial pair correlation functions $g_{\text{Ni-Al}}(r)$, $g_{\text{Ni-Ni}}(r)$ are plotted for Ni-Al and Ni-Ni pairs, respectively. The absence of second-nearest-neighbor peaks and the broadness of the other peaks are signatures of an amorphous phase. It is also seen that the integral of $g_{\text{Ni-Al}}(r)$ is larger than that of $g_{\text{Ni-Ni}}(r)$, even at the nearest-neighbor distance, indicating thorough mixing of Al substrate atoms with Ni cluster atoms. The average alloy concentration in the center of the amorphous impact zone is $\approx NiAl_2$. The pair correlation function of the Ni cluster, prior to impact, is shown for comparison. The broadness

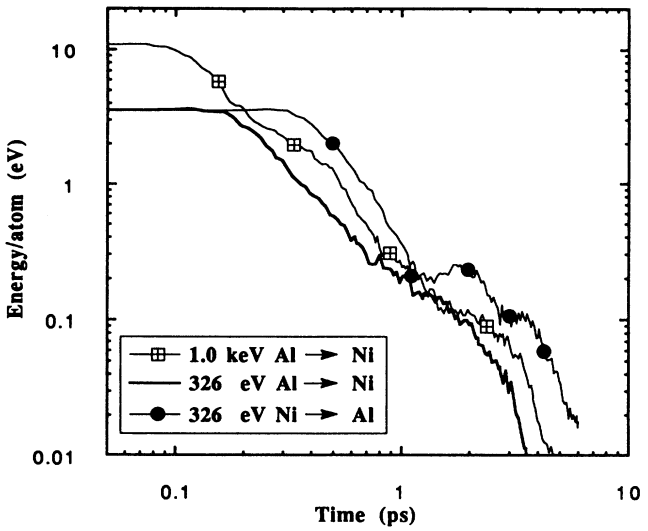

FIG. 12. Kinetic energies of cluster atoms as a function of time.

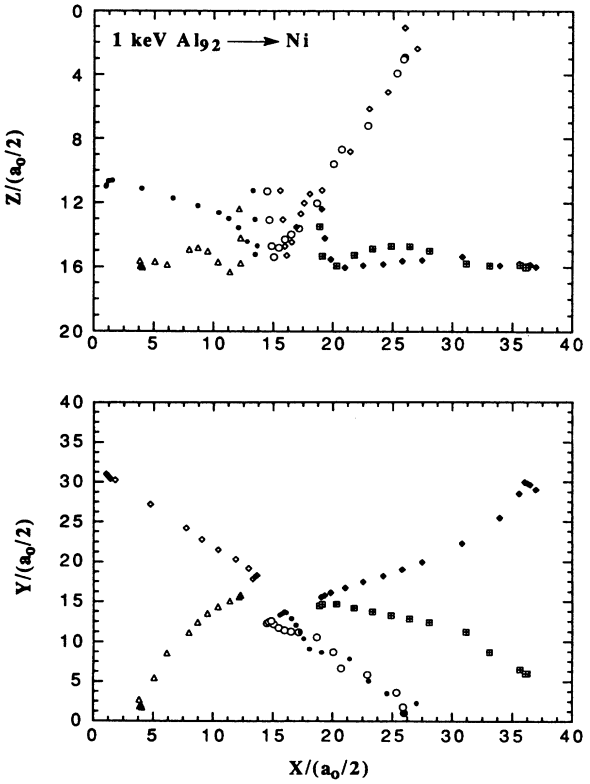

FIG. 11. Trajectories of some Al atoms that dissociate from the 1.0-keV Al cluster on impact with a Ni substrate. (a) Side view (upper); (b) top view (lower).

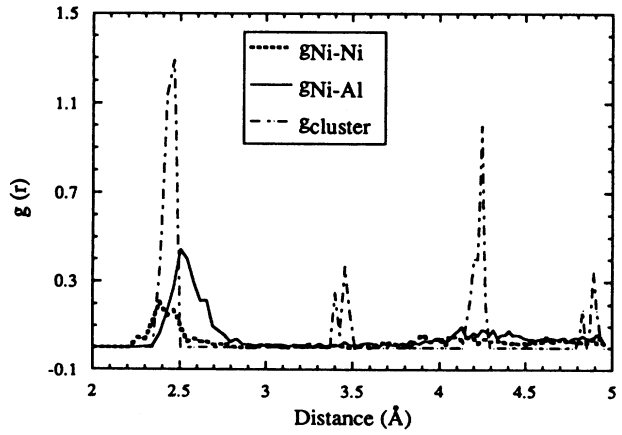

FIG. 13. Partial pair correlation functions for cluster atoms at the end of the Ni_{92}(326 eV)→event, and for the relaxed cluster before the collision begins.

of the peaks and peak splitting in this pure 92-atom cluster is a consequence of structural relaxation. The details of the mixing process have not yet been elucidated, but it appears that the cluster locally melts providing for the rapid interdiffusion. This is consistent with the kinetic energies in Fig. 12 and the low melting temperature of Al, 933 K. The energy for the melting can be supplied partially by the kinetic energy of the cluster and partly by the heat of solution, the latter being $\Delta H_{\rm sol}=145$ eV/92-atom cluster (the difference in the potential energy of the system at the beginning and end of the event).

V. CONCLUSIONS

The MD simulations described here show that the interaction of energetic clusters of atoms with solid surfaces can display a variety of different phenomena depending on several cluster-substrate parameters. These interactions are summarized in Fig. 14 by a "mechanism diagram." At the top of the diagram, when the kinetic energy/atom in the cluster $E^{\rm cl}_{\rm kin}/N_{\rm cl}$ is greater than about ten times the cohesive energy of the substrate, $E^{\rm sub}_{\rm coh}$, the threshold energy for atomic displacements is exceeded, and RCS's are generated. In addition, the cluster is implanted. This was illustrated by the smaller Cu clusters on Cu. At low cluster energies, the cluster remains intact, either forming a "glob" on the surface, if the substrate is hard, or penetrating it, if it is soft. At intermediate cluster energies, the cluster will break up if it strikes a hard substrate, either splatting, dissociating and migrating over, or being reflected from the surface. If the cluster strikes a soft substrate, it will penetrate it and induce local melting as it is stopped.

Since the relevant parameter space describing the interactions is more than two dimensional, this diagram represents a slice through a more complete diagram. Consequently, the choice of axes is somewhat arbitrary. As mentioned previously, and in the Appendix, the penetration of the cluster into the substrate is better described by the shear modulus of the substrate than by its cohesive energy; however, to reflect the importance of the relative properties of the substrate and cluster on the abscissa by a simple physical ratio, the cohesive energy was chosen. The diagram, therefore, is an approximate guide for the case of clusters in the size range $\approx 10-100$ atoms, energies between ≈ 50 and 5000 eV, and mass ratios of 0.5–2. Moreover, since only four cluster-substrate combinations were simulated, the diagram spans a larger region in this two-dimensional space than we have actually investigated.

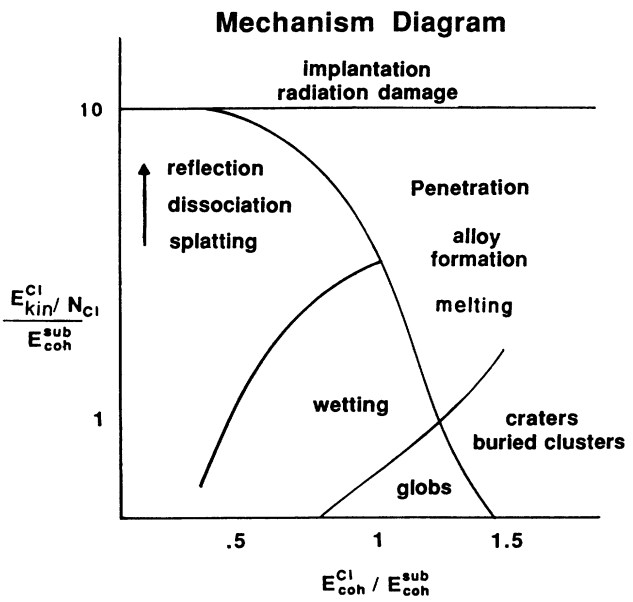

FIG. 14. Mechanism diagram of the interaction between energetic clusters of atoms and metal substrates.

Comparison of this chart with that in the Appendix reveals that the general behavior predicted by the macroscopic model is indeed observed. However, these atomistic simulations are important for locating the boundaries for different mechanisms and elucidating the details of the interactions along them. As it was demonstrated, rather small changes in certain parameters, e.g., the relative cohesive energies of the cluster and substrate, completely change the nature of the interaction. The macroscopic model does not show how sharp these boundaries actually are.

Much of the reported work on cluster beam deposition has been concerned with growing high-quality metallic films on Si substrates.[2] Yamada and coworkers reported that ionized cluster beam deposition is particularly useful for growing Al films on Si.[2] Moreover, they have shown, using masking techniques, that if the deposition is performed at room temperature, the Al atoms migrate far from the impact sites. The energy of these clusters were 0–5 keV. Unfortunately, the size distribution of the clusters employed in the Yamada experiments is not accurately known; however, if we guess they are in the range 50–1000, then their deposition conditions should resemble our simulations of Al_{92}(1 keV)$\rightarrow$Ni, since the cohesive energies of Ni and Si are rather similar (Table IV). In addition, since the ratio $E^{\rm cl}_{\rm coh}/E^{\rm sub}_{\rm coh}$ is less than one, little penetration is expected, and so differences in the chemical properties of Ni and Si should not be overly important for the collision dynamics. Inspection of the mechanism diagram, and Figs. 9(c) and 10(c) above for the Al on Ni impacts, shows that the Yamada experiments are in the regime of cluster "splatting" and dissociation. If single Al atoms are mobile on the Si surface at the deposition temperature, then the spreading of the Al beam "under the mask" is expected, as reported. If the cluster sizes were less than ≈ 25 atoms, then the ionized fraction of this beam would have an energy greater than 25 eV/atom (for cluster energies greater than ≈ 1 keV) and would create radiation damage in the Si substrate, probably creating a thin amorphous layer. This is not observed, perhaps indicating that the Yamada experiments do, indeed, involve large clusters. However, if the ionized fraction is extremely small and only single atoms or small clusters are deposited on the surface, the same results might also occur. The simulations, therefore, cannot verify whether the Yamada experiments have been

correctly interpreted; they are, however, consistent with this interpretation. If other combinations were experimentally examined, e.g., a hard cluster on a soft substrate, the characteristics of the cluster beam could be deduced from the simulations.

ACKNOWLEDGMENTS

The authors wish to acknowledge the help of Professor J. B. Adams on the retrieval of EAM potentials. The work was supported by the U.S. Department of Energy (Office of Basic Energy Science), under Grant No. DEFG02-91ER45439 through the Materials Research Laboratory of the University of Illinois at Urbana-Champaign (UIUC). Grants of computer time from the National Center for Supercomputing Applications at UIUC, and from the U.S. National Aeronautics and Space Administration (NASA) Ames Research Center are also gratefully acknowledged.

APPENDIX: GLOBAL DYNAMICS OF CLUSTER BEAM DEPOSITION

When modeled in macroscopic terms, the behavior of clusters during deposition has much in common with planetary cratering and armor penetrating ordinance. Here we first pursue the macroscopic model before finally commenting on its relevance.

We are concerned with regimes of behavior when a moving compact cluster impacts on an initially flat surface. Interesting phenomena span many orders of magnitude in cluster size and energy, while the relevant material properties scale into a relatively limited range, in which typical cases differ from the mean by a factor of order unity. In the impact, the kinetic energy of the incident cluster is converted into heat mainly by plastic deformation of the surface and of the cluster. A cluster of N atoms, radius $r=aN^{1/3}$, with a the atomic radius, when embedded in the surface, cools with time constant $\tau_D=r^2/D$, with D the heat diffusion coefficient, typically ≈ 0.1 cm^2/sec for $T>\Theta$, and Θ the Debye temperature. Thus, for $N\leq 200$, the cooling time

$$\tau_D \approx 3\times 10^{-15} N^{2/3} \tag{A1}$$

is less than one atomic vibrational period $\nu^{-1}=h/k\Theta\approx 10^{-13}$ sec. Such rapid cooling is not compatible with surface smoothing by solid-state diffusion, which typically requires 10^4 vibrations per jump, even for surface diffusion at the melting point T_m. Therefore, the final surface profile is determined by the plastic flow, unless the material exhibits local melting.

The melting of an initially cold cluster requires heat of order $3NkT_m$. By equating this to the initial kinetic energy of N atoms of mass M and velocity v we obtain the necessary critical velocity as

$$v=(12kT_m/M)^{1/2}\approx(T_m/10\mu)^{1/2}\ \text{km/sec}\ , \tag{A2}$$

with μ the mass number and T_m in K. For $T_m\approx 1000$ K and $\mu\approx 100$, the magnitude of the resulting velocities ≈ 1 km/sec is clearly that of meteorite and missile impacts. A factor of 2 in the energy has been included to account for comparable heating of surface material.

To assess the time scale of the events further we estimate the duration τ of the impact. When the cluster embeds itself to depth r in the surface with initial velocity v, the impact time is clearly of order $\tau\approx r/v$, which, using values of the critical velocity for melting, gives

$$\begin{aligned}\tau &\approx 10^{-8}N^{1/3}/10^5(10\mu/T_m)^{1/2}\\ &\approx 10^{-13}N^{1/3}(10\mu/T_m)^{-1/2}\ .\end{aligned} \tag{A3}$$

With the last factor ≈ 1, this impact time exceeds the cooling time by a factor of $30/N^{1/3}$, which falls to unity only for $N\geq 10^4$ atoms. It is therefore evident that much heat energy is lost from the location of the impact *during* the collision, for events with $N\leq 10^4$ typically of interest in cluster beam deposition.

In summary, the results of these estimates indicate that plastic deformation and melting, rather than solid-state diffusion, determine the surface profile after the event. Melting requires a kinetic energy associated with initial cluster velocities $\approx$km/sec. The resulting impact times for $N<10^4$ are, however, longer than the time constant for cooling by thermal conduction. Consequently, the impact energies required for actual melting are larger that would otherwise be expected. The situation is further complicated by the fact that the cooling time is comparable with the atomic vibrational period in this regime.

An approximate description of the plastic processes during the impact may now be obtained in the following way. Suppose that the cluster and the surface exert on each other a mean force F for the duration τ of the collision. The cluster and the surface undergo comparable deformations corresponding to similar accelerations μ/τ and s/τ^2, respectively, with $\tau\approx s/v$. F and s are related to the energy E of the incident cluster by $E=Fs$, and the force defines a shear stress σ by $\sigma\approx F/\pi r^2$. Supposing that during the impact the stress rises to a critical value and then remains approximately constant: we find, by eliminating F, the results $s=E/\pi r^2\sigma=Er/\sigma N\Omega$, in which Ω is the volume per atom. The fractional deformation now becomes

$$s/r=E/N\sigma\Omega=f\varepsilon/\sigma\Omega,\quad s\leq r\ . \tag{A4}$$

Here we have expressed the cluster kinetic energy $E=Nf\varepsilon$ as a fraction f of the cohesive energy ε per particle. Rather good approximations to other relevant quantities for typical crystals in these same terms are

$$\varepsilon\approx 10c\Omega\approx 30kT_m\ ,$$

in which c is a mean shear modulus.

A phase diagram describing the impact in terms of N and f can thus be conceived in which, for example, melting occurs for $f\approx 0.2$ independent of $N<$ if cooling is neglected. Similarly $N\approx 200$ when $s/r\approx 1$ is the condition for the cooling time to fall below one Debye period. The fractional deformation becomes $s/r=(10c/\Omega)f$. Consequently the boundary for deep cratering of the surface, corresponding to $s/r\approx 1$, occurs for

$$f\approx\sigma/10c\ . \tag{A5}$$

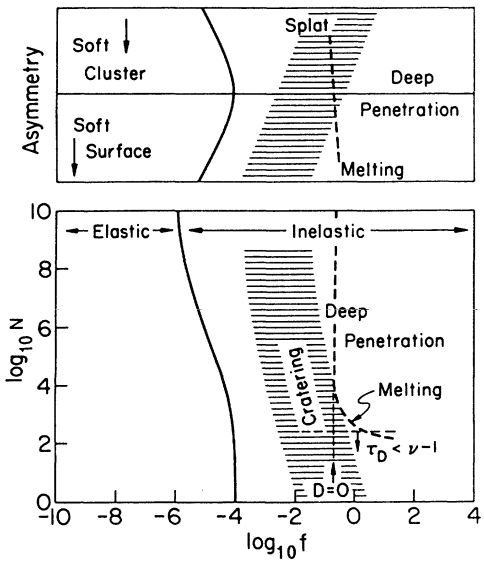

FIG. 15. Schematic phase diagram of the cluster-surface interaction.

In microscopic systems, the critical yield stress may approach c, and this limit may be reached at $N \approx 10^3$. For larger systems, the ratios s/c is much reduced by dislocation processes. The several deductions are included in the schematic phase diagram of Fig. 15, including the fact that deep cratering for smaller clusters almost coincides with the melting criterion for $D=0$. The approximate regime of elastic collisions is also indicated.

Two main points become clear when these results are assessed. First, the actual cluster beam behavior, in the interesting regime where a tendency to smooth growth may arise, is quite complex, because the impact, the heat transfer, and the atomic vibrations all occur on similar time scales. Macroscopic modeling cannot provide details of these processes, for which molecular-dynamics computations are very well suited. Second, what the present modeling does provide is a conceptual framework in which recognizable regimes of behavior are identified, as in Fig. 15. In turn, these point to "phase boundaries," at which the behavior changes, as regions of particular interest for detailed dynamical simulations. To illustrate this further, we note that interesting complications occur when the cluster and surface materials differ. The asymmetry introduced by significant differences of melting point or of yield stress for the two materials necessarily give rise to new behavior in the form of liquid splattering of the cluster or of added deep penetration by the cluster in the two limits of soft or hard clusters. These differences are sketched in the top part of Fig. 15.

We note, in conclusion, that the heat flow of critical interest here occurs in the regime near T_m of small-phonon mean-free paths, where the macroscopic model can reasonably be applied to phenomena on a nm length scale. Similarly, the mechanical phenomena of forces and pressures are reasonably well defined over the areas of 10^2 atoms. For these reasons, there is no reason to suppose that the macroscopic analogy used here is qualitatively misleading.

*Present address: General Physics International, 6700 Alexander Bell Drive, Columbia, Maryland 21046.

[1]*Proceedings of the Second International Workshop on MeV and keV Ion and Cluster Interactions with Surfaces and Materials* [Colloq. Phys., Colloq. No. 2 (1989)].

[2]I. Yamada, Appl. Surf. Sci. **43**, 23 (1989).

[3]Y. Yamamura, I. Yamada, and T. Takagi, Nucl. Instrum. Methods B **37/38**, 902 (1987).

[4]R. J. Buehler, G. Friedlander, and L. Friedman, Phys. Rev. Lett. **63**, 1292 (1989).

[5]See, e.g., *Beam-Solid Interactions and Transient Processes,* edited by M. O. Thompson, S. T. Picraux, and J. S. Williams, MRS Symposia Proceedings No. 74 (Materials Research Society, Pittsburgh, 1987).

[6]H. Hsieh and R. S. Averback, Phys. Rev. B **42**, 5365 (1990).

[7]H. Hsieh, R. S. Averback, and R. Benedek, in *Beam-Solid Interactions: Physical Phenomena,* edited by J. A. Knapp *et al.*, MRS Sympsia Proceedings No. 157 (Materials Research Society, Pittsburgh, 1990).

[8]S. M. Foiles, M. I. Baskes, and M. S. Daw, Phys. Rev. B **33**, 7983 (1986).

[9]S. P. Chen, A. F. Voter, R. C. Albers, A. M. Boring, and P. J. Hay, J. Mater. Res. **5**, 955 (1990).

[10]J. Almlof, K. Faegri, Jr., and K. Korsell, J. Comput. Chem. **3**, 385 (1982).

[11]J. F. Ziegler, J. P. Biersack and U. Littmark, *The Stopping and Ranges of Ions in Solids* (Pergamon, New York, 1985).

[12]W. E. King and R. Benedek, J. Nucl. Mater. **117**, 26 (1983).

[13]J. B. Gibson, A. N. Goland, M. Milgram, and G. H. Vineyard, Phys. Rev. **120**, 1229 (1960).

[14]H. Hsieh, H. Sellers, and R. S. Averback, unpublished.

[15]T. Diaz de la Rubia, R. S. Averback, R. Benedek, and W. E. King, Phys. Rev. Lett. **59**, 1930 (1987).